Positronium formation for positron scattering from hydrogen: Maximum positions and scaling law

L. Jiao, Y. Wang, and Y. Zhou

Center for Theoretical Atomic and Molecular Physics, Academy of Fundamental and Interdisciplinary Sciences, Harbin Institute of Technology, Harbin 150080, People's Republic of China

(Received 25 September 2011; published 14 November 2011)

Ground- and excited-state positronium (Ps) formation from the hydrogen atom by positron impact at low and intermediate energies have been studied within the framework of two-center two-channel eikonal final state-continuum initial distorted wave model. A general method for obtaining Ps formation into arbitrary final states has been derived. The present results of Ps ($1s$), Ps ($n = 2$), and total Ps formation cross sections agree very well with previous close-coupling calculations and experimental measurements. The maximum positions of Ps(n) formation cross sections are found to be in good agreement with the prediction of wave vector matching model introduced by Charlton [J. Phys. B **39**, 4575 (2006)]. We also present a scaling law for Ps (n) formation cross sections that is valid for all n in the entire energy range.

DOI: 10.1103/PhysRevA.84.052711 PACS number(s): 34.70.+e, 34.80.Uv, 36.10.Dr

I. INTRODUCTION

Positronium (Ps) formation is one of the most important quantal rearrangement collisions that can occur in nature and it has attracted much attention in both theoretical and experimental studies over the past two decades [1,2]. For the simplest case of positron-hydrogen collision, the experimental measurement of Ps formation cross section is now amenable and reliable results have been obtained [3,4]. On the theoretical side, the Ps formation process has been widely investigated by several perturbation methods, such as the first- and second-order Born (FBA and SBA) [5,6], first and second distorted-wave approximations (DWA and SDWA) [7,8], polarized-orbital distorted-wave approximation (PODWA) [9,10], and the continuum distorted-wave (CDW) [11-14] methods. The more elaborate close-coupling (CC) methods have also been successfully applied to investigate the Ps formation process in positron-hydrogen collision. These calculations include the CC (9,9) and CC (30,3) models of Kernoghan *et al*. [15], CC (28,3) of Mitroy [16], hyperspherical coupled-channel (HSCC) of Igarashi *et al*. [17], time-dependent coupled-channel (TDCC) of Yamanaka *et al*. [18], convergent close-coupling (CCC) of Kadyrov *et al*. [19], and coupled-channel optical (CCO) method of Cheng and Zhou [20]. Some other state-of-the-art methods [21–24] have also been applied to this process and satisfied results are obtained.

By comparing these theoretical calculations and the experimental observations, good agreement has been achieved for the ground and total Ps formation cross sections. However, different situations arise for excited-state Ps formations. A large discrepancy exists among calculations performed by different methods in the case of Ps ($n = 2$) formation. Moreover, few calculations have been performed for higher excited-state Ps formations. Recently, Ghoshal *et al*. [25] have successfully applied the DWA method to study the transition of arbitrary hydrogen s state to arbitrary Ps s state. A general formalism to obtain Ps formation cross sections for all reactions has been derived in the intermediate and high energy range. However, it is known that the DWA theory is not very accurate at low energies and further investigations are still required to shed light on this area.

As a typical example of asymmetric charge transfer processes, the Ps formation at which it is most likely to occur is a long-term research subject [26]. The recent study of Charlton [27] based upon wave vector matching model has shown that "*for positron collisions with a wide variety of targets, cross sections for positronium formation are largest when the projectile kinetic energy is in the vicinity of twice the relevant threshold energy.*" In the case of hydrogen atom, the Ps ($1s$) formation peak located at 13–14 eV has already been predicted by various theoretical work and identified by experiments. Therefore, it is very interesting to investigate whether the excited Ps formations follow such criterion.

In this paper, we employ the eikonal final state-continuum initial distorted wave (EFS-CDW) model to calculate arbitrary excited-state Ps formation from the ground state of hydrogen by positron impact. The continuum distorted wave method was originally proposed by Cheshire [28] to deal with ion-atom charge exchange collision. With continuous development by theorists in the past years, the two-center CDW models have been successfully applied to light projectile collisions [29–32]. The pioneering work on the Ps formation process by positron impact on hydrogen atom using the two-center two-channel distorted-wave EFS-CDW approximation has been performed by Macri *et al*. [13,14]. It has been shown that the perturbative EFS-CDW model can be successfully extended to the low-energy range. In this work, we go a step further and develop a full EFS-CDW model to calculate the arbitrary excited-state Ps formation by positron impact on hydrogen atom. By summing the Ps (nlm) formation cross sections with quantum numbers l,m and then n, we have obtained the Ps (n) and total Ps formation cross sections and compared them with other theoretical calculations and experimental measurements. Finally, we pay extreme attention to the maximum position and the scaling law for Ps (n) formation cross sections. A general trend for the scaling factor is given to ensure the validity of the scaling law in the entire energy range investigated.

II. THEORY

A. General EFS-CDW formalism

In the distorted-wave formalism, the prior form of the exact transition matrix (T matrix) element is given by the two-potential formula of Gell-Mann and Goldberger [33]:

$$T_{fi} = \langle \Psi_f^{(-)} | W_i | \chi_i^{(+)} \rangle + \langle \Phi_f | V_f^{\dagger} - W_i | \chi_i^{(+)} \rangle. \quad (1)$$

Here $\Psi_f^{(-)}$ is the exact scattering wave function developed from the final asymptotic state satisfying exact ingoing-wave $(-)$ boundary conditions, $\chi_i^{(+)}$ is a distorted wave developed from the initial asymptotic state satisfying exact outgoing-wave $(+)$ boundary conditions but is otherwise arbitrary (W_i is the corresponding perturbation). Φ_f is the unperturbed final state and V_f is the final-state channel interaction.

In the EFS-CDW model, the initial and final states are given by

$$\chi_i^{(+)\mathrm{CDW}} = \Phi_i^B(\mathbf{R}_P,\mathbf{r}_T) F^{(+)}(a_P, -\mu \mathbf{v}_i, \mathbf{r}_P) \times F^{(+)}(a_i, \mathbf{v}_i, \mathbf{R}) \mu^{-i a_P}, \quad (2)$$

$$\Psi_f^{(-)\mathrm{EFS}} = \Phi_f^B(\mathbf{R}_T,\mathbf{r}_P) E^{(-)}(a_T, \mathbf{v}_f, \mathbf{r}_T) E^{(-)}(a_f, \mathbf{v}_f, \mathbf{R}). \quad (3)$$

The paris of Jacobi coordinates $(\mathbf{r}_T,\mathbf{R}_P)$, $(\mathbf{r}_P,\mathbf{R}_T)$, and $(\mathbf{R},\mathbf{r})$ are used to describe the three-particle system (see, for example, Ref. [13]). $\mathbf{v}_{i,f}$ are the incoming positron and outgoing Ps velocities and $\Phi_{i,f}^B$ are the asymptotic initial and final states. $F^{(+)}$ and $E^{(-)}$ are the continuum distorted and eikonal phase factors, which represent the distortion effects of the Coulomb potentials in the entry and exit channels, respectively. $a_{P,i}$ and $a_{T,f}$ are the corresponding Sommerfeld factors. Here we should note that the factor $\mu^{-i a_P}$ (with $\mu = 1/2$, the reduced mass of positron to electron) is needed so that the initial-state wave function asymptotically goes over to the unperturbed initial state [34].

The perturbation W_i is the difference between the exact initial-state interaction between all three particles and the approximate scattering potential used to calculate χ_i^{CDW}:

$$W_i \chi_i^{\mathrm{CDW}} = \left(\frac{1}{M_P} \nabla_{\mathbf{r}_P} \cdot \nabla_{\mathbf{R}} - \frac{1}{M_T} \nabla_{\mathbf{r}_T} \cdot \nabla_{\mathbf{R}} - \frac{1}{m} \nabla_{\mathbf{r}_T} \cdot \nabla_{\mathbf{r}_P} \right) \chi_i^{\mathrm{CDW}}, \quad (4)$$

where M_P, m, and M_T are the positron, electron, and target nucleus mass, respectively. The channel interaction for final state Φ_f^B is

$$V_f = 1/R - 1/r_T. \quad (5)$$

Following the computational method introduced by Macri *et al.* [13], we use a Fourier transformation for the electron to positron coordinate $\mathbf{r}_P$ and then integrating the coordinates $\mathbf{r}_T$ and $\mathbf{R}$ separately. Finally, the six-dimensional numerical quadrature can be reduced to three-dimensional ones. The final form of the T matrix elements are written as follows:

$$T_{fi}^{\mathrm{EFS-CDW}} = T_1^{\mathrm{EFS-CDW}} + T_2^{\mathrm{EFS-CDW}}, \quad (6)$$

$$T_1^{\mathrm{EFS-CDW}} = \int \frac{d\mathbf{Q}}{(2\pi)^{3/2}} \{ \widetilde{\mathbf{G}}(\mathbf{Q}) \cdot [\boldsymbol{J}_{TP}(\mathbf{Q}) I_T(\mathbf{Q}) - \mathbf{J}_T(\mathbf{Q}) I_{TP}(\mathbf{Q})] - \frac{\widetilde{F}(\mathbf{Q})}{M_T} [\mathbf{J}_{TP}(\mathbf{Q}) \cdot \mathbf{J}_T(\mathbf{Q})] \}, \quad (7)$$

$$T_2^{\mathrm{EFS-CDW}} = \int \frac{d\mathbf{Q}}{(2\pi)^{3/2}} \{ \widetilde{F}(\mathbf{Q}) [N_{TP}(\mathbf{Q}) M_T(\mathbf{Q}) - N_T(\mathbf{Q}) \times M_{TP}(\mathbf{Q})] \} - T_1^{\mathrm{EFS-CDW}} \Big|_{(a_T = a_f = 0)}, \quad (8)$$

where the Fourier transformations are

$$\widetilde{\mathbf{G}}(\mathbf{Q}) = \int \frac{d\mathbf{r}_P}{(2\pi)^{3/2}} e^{(i\mathbf{Q}\cdot\mathbf{r}_P)} \phi_f^*(\mathbf{r}_P) \nabla_{\mathbf{r}_P} F^{(+)}(a_P, -\mu \mathbf{v}_i, \mathbf{r}_P), \quad (9)$$

$$\widetilde{F}(\mathbf{Q}) = \int \frac{d\mathbf{r}_P}{(2\pi)^{3/2}} e^{(i\mathbf{Q}\cdot\mathbf{r}_P)} \phi_f^*(\mathbf{r}_P) F^{(+)}(a_P, -\mu \mathbf{v}_i, \mathbf{r}_P), \quad (10)$$

and the remaining vectorial and scalar integrals are

$$\mathbf{J}_{TP}(\mathbf{Q}) = \int d\mathbf{R} e^{[i(\mathbf{v}_i - \mathbf{v}_f + \mathbf{Q})\cdot\mathbf{R} - \epsilon R]} E^{(-)*}(a_f, \mathbf{v}_f, \mathbf{R}) \times \nabla_{\mathbf{R}} F^{(+)}(a_i, \mathbf{v}_i, \mathbf{R}), \quad (11)$$

$$\mathbf{J}_T(\mathbf{Q}) = \int d\mathbf{r}_T e^{[-i(\mathbf{v}_f + \mathbf{Q})\cdot\mathbf{r}_T]} E^{(-)*}(a_T, \mathbf{v}_f, \mathbf{r}_T) \nabla_{\mathbf{r}_T} \phi_i(\mathbf{r}_T), \quad (12)$$

$$I_{TP}(\mathbf{Q}) = \int d\mathbf{R} e^{[i(\mathbf{v}_i - \mathbf{v}_f + \mathbf{Q})\cdot\mathbf{R} - \epsilon R]} E^{(-)*}(a_f, \mathbf{v}_f, \mathbf{R}) F^{(+)}(a_i, \mathbf{v}_i, \mathbf{R}), \quad (13)$$

$$I_T(\mathbf{Q}) = \int d\mathbf{r}_T e^{[-i(\mathbf{v}_f + \mathbf{Q})\cdot\mathbf{r}_T]} E^{(-)*}(a_T, \mathbf{v}_f, \mathbf{r}_T) \phi_i(\mathbf{r}_T), \quad (14)$$

$$N_{TP}(\mathbf{Q}) = \int d\mathbf{R} e^{[i(\mathbf{v}_i - \mathbf{v}_f + \mathbf{Q})\cdot\mathbf{R} - \epsilon R]} \frac{1}{R} F^{(+)}(a_i, \mathbf{v}_i, \mathbf{R}), \quad (15)$$

$$N_T(\mathbf{Q}) = \int d\mathbf{r}_T e^{[-i(\mathbf{v}_f + \mathbf{Q})\cdot\mathbf{r}_T]} \frac{1}{r_T} \phi_i(\mathbf{r}_T), \quad (16)$$

$$M_{TP}(\mathbf{Q}) = \int d\mathbf{R} e^{[i(\mathbf{v}_i - \mathbf{v}_f + \mathbf{Q})\cdot\mathbf{R} - \epsilon R]} F^{(+)}(a_i, \mathbf{v}_i, \mathbf{R}), \quad (17)$$

$$M_T(\mathbf{Q}) = \int d\mathbf{r}_T e^{[-i(\mathbf{v}_f + \mathbf{Q})\cdot\mathbf{r}_T]} \phi_i(\mathbf{r}_T). \quad (18)$$

Here ϵ is a convergence factor and it takes the limit of 0^+ in the above integrations. Comparing with previous model of Macri *et al.* [13], we take into account the full interactions in Eq. (7) and the higher-order term of Eq. (8) in the present calculations. The first term of Eq. (8) is just the B-CDW model introduced by Chen *et al.* [11] and Bransden *et al.* [12], which can be understood from Eq. (1).

B. Ps formation into arbitrary states

To obtain the arbitrary excited-state Ps formation cross sections, one should calculate the Fourier transformations Eqs. (9) and (10), which exactly include the final Ps wave function. For calculating the T matrix elements of Eqs. (7) and (8) easily, the Z axis is taken along the incident positron

velocity $\mathbf{v}_i$ and the outgoing Ps velocity $\mathbf{v}_f$ is set in the XZ plane without generalization (see Fig. 1). For Ps formation in ground state, Eqs. (9) and (10) can be easily evaluated by using the Nordsieck integrals [35]. However, for Ps ($n \geqslant 2$) states, the angular part of the Ps wave function makes the calculation rather complicated due to the quantization axis of the final Ps state is along the vector $\mathbf{v}_f$ and the direction of the momentum $\mathbf{Q}$ introduced from the Fourier transformation is arbitrary. An alternative way to deal with this is rotating the coordinate system so that, in the final coordinate system, the quantization axis $\mathbf{v}_f$ becomes the Z axis. Subsequently, the Fourier transformation can be easily calculated in terms of the bound-free transition form factors.

First, by substituting the detailed continuum distorted wave factor into Eq. (9) and applying the gradient transformation of the confluent hypergeometric functions,

$$r\nabla_{\mathbf{r}1}F_1(ia,1,ipr+i\mathbf{p}\cdot\mathbf{r}) = p\nabla_{\mathbf{p}1}F_1(ia,1,ipr+i\mathbf{p}\cdot\mathbf{r}), \tag{19}$$

Eq. (9) takes the form

$$\widetilde{\mathbf{G}}(\mathbf{Q}) = pN_\beta\nabla_{\mathbf{p}}\int\frac{d\mathbf{r}_P}{(2\pi)^{3/2}}\phi^*_{nlm}(\mathbf{r}_P)\frac{e^{(i\mathbf{Q}\cdot\mathbf{r}_P)}}{r_P} \times {}_1F_1(i\beta,1,ipr_P+i\mathbf{p}\cdot\mathbf{r}_P), \tag{20}$$

where

$$N_\beta = \Gamma(1-i\beta)e^{\pi\beta/2},\ \mathbf{p}=\mu\mathbf{v}_i,\ \beta=-a_P. \tag{21}$$

Second, as shown in Fig. 1, we rotate the coordinate system about Y axis so that $\mathbf{v}_f$ becomes the new Z axis. To do this, the vectors $\mathbf{Q}$ and $\mathbf{p}$ should be transformed as

$$Q_{X'} = \mathscr{F}(Q_X,Q_Z,\theta),\ p_{X'} = \mathscr{F}(p_X,p_Z,\theta), \tag{22}$$

$$Q_{Y'} = Q_Y,\ p_{Y'} = p_Y, \tag{23}$$

$$Q_{Z'} = \mathscr{G}(Q_X,Q_Z,\theta),\ p_{Z'} = \mathscr{G}(p_X,p_Z,\theta), \tag{24}$$

where X,Y,Z is the old coordinate system, whereas X',Y',Z' refer to the new coordinate system. θ is the angle between axes Z and Z'. In the new coordinate system, Eq. (20) can

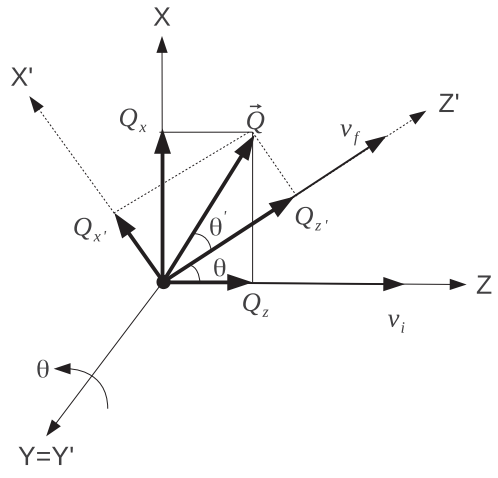

FIG. 1. Transformation of the coordinate system about Y axis. X,Y,Z: old frame; X',Y',Z': new frame. $\mathbf{v}_i$ and $\mathbf{v}_f$ are the incoming positron and outgoing Ps velocities, respectively. Details are described in the text.

be readily calculated by employing the bound-free transition form factors of Belkic [36]:

$$\widetilde{\mathbf{G}}'(\mathbf{Q}',\mathbf{p}') = \frac{(-1)^m p'}{(2\pi)^{3/2}}\nabla_{\mathbf{p}'}\mathbf{A}^{(\mathbf{v}_f)}_{\alpha\beta}(0,0,\mathbf{Q}'+\mathbf{p}';nl\text{-}m,\mathbf{p}'), \tag{25}$$

where the factor $\mathbf{A}^{(\mathbf{v}_f)}_{\alpha\beta}$ is given by Eq. (21) in Ref. [36] with α the usual exponential parameter associated with the orbital $\langle\mathbf{r}|nl\text{-}m\rangle$. $Z_\alpha = 1/2$ is used to ensure the hydrogenic wave functions for Ps atom.

At last, before substituting Eq. (25) into the T matrix element Eq. (7), we should rotate the coordinate system back, which can be achieved by making an inverse transformation from $\widetilde{\mathbf{G}}'(\mathbf{Q}',\mathbf{p}')$ to $\widetilde{\mathbf{G}}(\mathbf{Q},\mathbf{p})$. The Fourier transformation $\widetilde{F}(\mathbf{Q},\mathbf{p})$ is analogous to $\widetilde{\mathbf{G}}(\mathbf{Q},\mathbf{p})$ without the gradient operator.

The differential and integral Ps (nlm) formation cross sections are given by

$$\frac{d\sigma_{Ps}(nlm)}{d\Omega} = \frac{1}{2\pi^2}\frac{v_f}{\mu v_i}|T_{fi}(nlm)|^2, \tag{26}$$

$$\sigma_{Ps}(nlm) = 2\pi\int_0^\pi\frac{d\sigma_{Ps}(nlm)}{d\Omega}\sin\theta d\theta. \tag{27}$$

The partial Ps (n) and total Ps formation cross sections are

$$\sigma_{Ps}(n) = \sum_{l=0}^{n-1}\sum_{m=-l}^{l}\sigma_{Ps}(nlm), \tag{28}$$

$$\sigma_{Ps} = \sum_n\sigma_{Ps}(n). \tag{29}$$

III. RESULTS AND DISCUSSION

A. Ps(1s) formation and the convergence of calculations

In the present calculations, the integrals of Eqs. (11)–(18) are all calculated in the analytical form and the final three-dimensional integration about $\mathbf{Q}$ in Eqs. (7) and (8) are evaluated numerically by the globally adaptive algorithm of Cuhre [37]. Cross check with several Monte-Carlo methods [37] has also been done to make sure the integration is accurate with error less than 1%. Another aspect that affects the integration accuracy is the convergence factor ϵ. We have calculated the Ps (1s) formation cross section at 14 eV impact energy and 0° emission angle with various ϵ and the results are shown in Fig. 2. Although the calculations are time-consuming with very small ϵ, good convergence can be achieved if more than 5×10^6 points are used in the three-dimensional quadratures. As we can see from Fig. 2, the results linearly approach to the limit where $\epsilon = 0^+$ and the convergence factor ϵ should be at least less than 0.001 to make sure the calculation uncertainty is less than 1%. In the following calculations, $\epsilon = 0.0005$ is used for all integrations.

In Fig. 3, we display the Ps (1s) formation cross sections below 100 eV. The present results are in excellent agreement with the CC (28,3) of Mitroy [16], CC (30,3) of Kernoghan *et al.* [15], HSCC of Igarashi *et al.* [17](not shown here for clarity), and CCO method of Cheng *et al.* [20]. The CCC results of Kadyrov *et al.* [19] and CC (9,9) results are slightly higher than present calculations. By omitting the higher-order terms, reducing the interaction potential of Eq. (4) and employing $\epsilon = 0.005$, we reproduce previous EFS-CDW

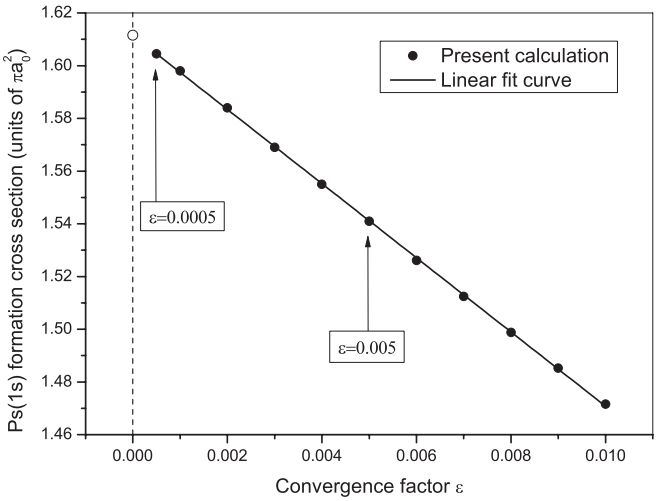

FIG. 2. Convergence of present calculations about the Ps ($1s$) formation cross sections at 14 eV impact energy and 0 degree emission angle. The open circle represents the presumable result at the limit $\epsilon = 0^+$.

calculations of Macri *et al.* [13]. It can be seen that their results are smaller than the present as well as these CC results, especially at the maximum position. Several other perturbation methods are also included in this figure. The DWA [7] model overestimates the Ps formation significantly at low energies, while the PODWA [9] underestimates it. The distorted-wave calculations are expected to be more reliable at relatively high energies. The peak position of the Ps ($1s$) formation cross sections can be clearly seen from this figure. The present EFS-CDW and the CC models all predict the maximum nearly at 13.8 eV, which is almost twice the relevant threshold energy of 6.8 eV.

B. Ps ($n \geqslant 2$) formations and the maximum positions

Due to degeneracy of the states of Ps atom with same principal quantum number n, we pay particular attention to the summed Ps (n) formation cross sections to investigate the relationship between the maximum positions and relevant

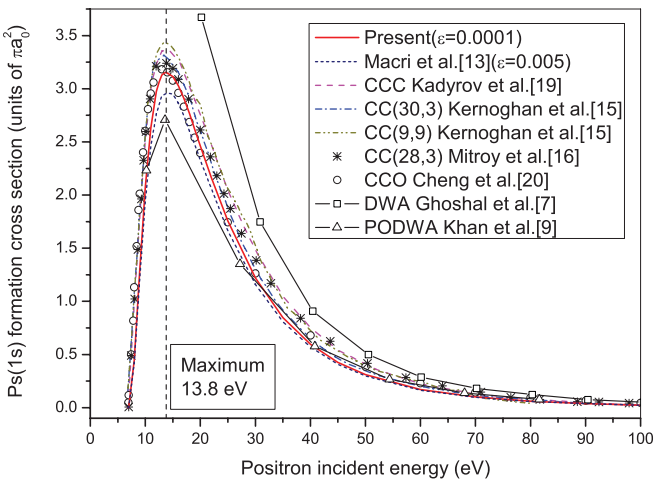

FIG. 3. (Color online) Ps ($1s$) formation cross sections for positron-hydrogen scattering.

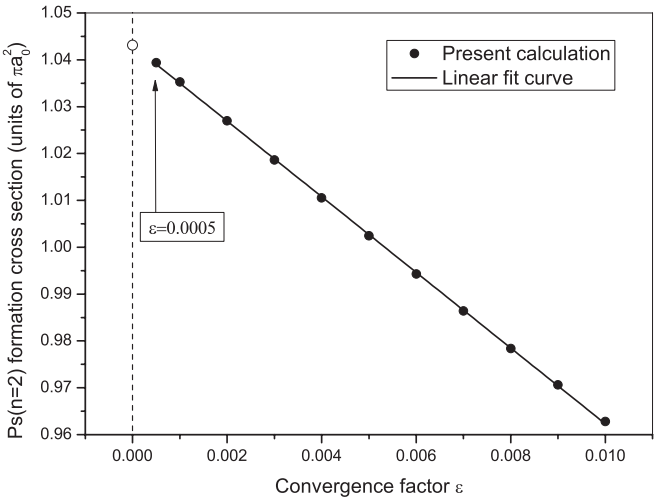

FIG. 4. The same as described in the legend of Fig. 2 but for Ps ($n = 2$) formation cross sections at 30 eV impact energy and 0° emission angle.

formation thresholds. The convergence of the present calculations about Ps ($n = 2$) formation cross sections has been studied and the results are displayed in Fig. 4. The use of $\epsilon = 0.0005$ shows that the uncertainty of our calculations is less than 0.5%. The present integrated cross sections for the first excited Ps ($n = 2$) formation are shown in Fig. 5 along with other theoretical results for comparison. The present EFS-CDW model shows a distinct maximum at 23.2 eV, which is in fairly good accordance with the CCC calculations of Kadyrov *et al.* [19], although the present results are higher than their results in the maximum region. The CC (30,3) and CC (9,9) models of Kernoghan *et al.* [15] show a better agreement with present calculations in magnitude. However, their calculations have some oscillations at the peak position and the exact maxima are hard to estimate. It is also very

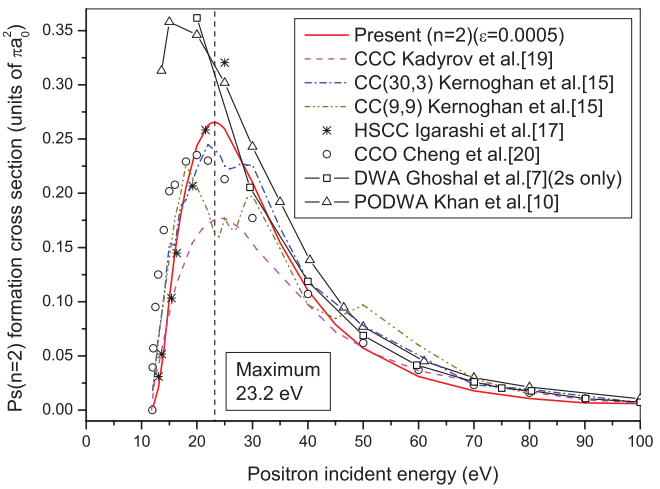

FIG. 5. (Color online) Ps ($n = 2$) formation cross sections for positron-hydrogen scattering. The CC (9,9), CC (30,3), CCC, and PODWA results are obtained by summing the corresponding Ps($2s$) and Ps($2p$) formation cross sections. The DWA results are only available for Ps ($2s$) formation. The HSCC results are drawn from Fig. 7 in Ref. [17].

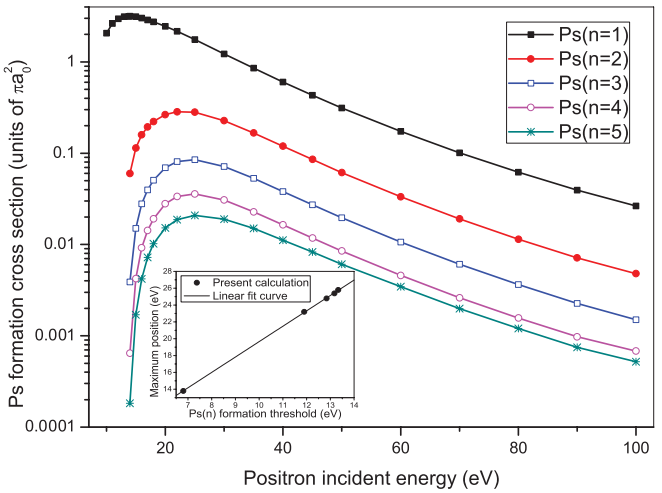

FIG. 6. (Color online) Ps ($n = 1 - 5$) formation cross sections for positron-hydrogen scattering.

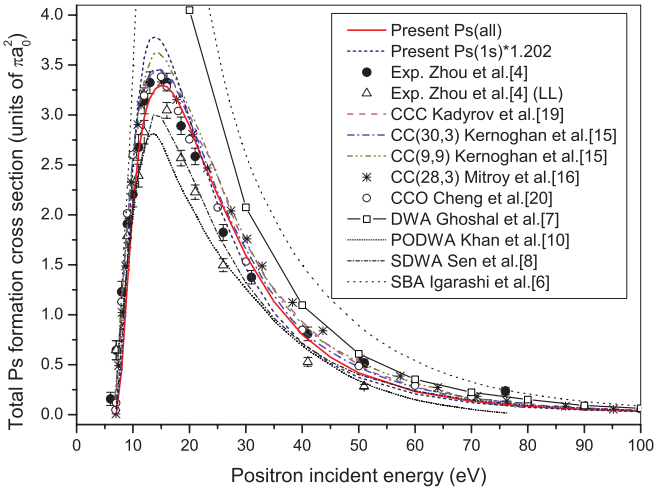

FIG. 7. (Color online) Total Ps formation cross sections for positron-hydrogen scattering.

interesting to compare these results among CC models. The CC (30,3) results are slightly larger than the predictions of CC (9,9) and CCC models due to the exclusion of higher Ps formation channels that are open in this energy region. The CC (9,9) model has a significant drop at the maximum, probably because such coupling scheme is not yet convergent. The two-center convergent close-coupling approach to the Ps formation process is carried out by expanding the total scattering wave function with sufficient number of states centered separately on the hydrogen atom and Ps [19]. Their results give the most convergent and stable cross sections compared with other CC models and achieve the maximum around 24 eV, which is in reasonably good agreement with present calculations. It is not surprising that the present calculations give larger results than the CCC and CC (9,9) models in the proximity of maximum due to the uncoupling character of the EFS-CDW model. The agreement of present results with the CCO [20] model is also very good except that they predict the maximum at relatively lower energy. The HSCC [17] results for Ps ($n = 2$) formation are only available at relatively low energies. As seen from the figure, the present results accord with their calculations very well at energies below 23 eV. The results of PODWA [10] and DWA [7] (only $2s$) models are also shown in this figure. As in the process of Ps($1s$) formation, the DWA model overestimates the cross sections at low-energy range. The PODWA results increase significantly as the energy decreases and achieve the maximum close to the Ps ($n = 2$) formation threshold.

In Fig. 6, we show the cross sections for the lowest five excited Ps (n) formations. For such highly excited Ps formations, the states with lower angular and magnetic quantum numbers, l and m, dominate the cross sections. Thus we only include the states with $l \leqslant 2$ and $|m| \leqslant 1$ in Eq. (28). The peak positions of the cross sections for Ps ($n = 3 - 5$) formations calculated in the present EFS-CDW model are 24.8, 25.4, and 25.8 eV with the corresponding thresholds at 12.84, 13.17, and 13.33 eV, respectively. It has recently been clarified by Charlton [27] that the charge exchange reaction of Ps formation is most likely when the wave vectors of the incoming positron and the outgoing Ps are matched; i.e., the positron and Ps de Broglie wavelengths are equal. This wave vector matching model implies that the Ps formation cross sections are largest when the projectile energy is in the vicinity of twice the relevant threshold energy. As displayed in the embedded figure in Fig. 6, the linearly fitting line to the peak positions versus the formation thresholds has a gradient of 1.83, which accords with the wave vector matching prediction of 2 reasonably well. We predict theoretically that such criterion is still valid for highly excited Ps formations.

C. Total Ps formation and the scaling law

By summing the Ps (n) formation cross sections with $n \leqslant 5$, we can approximately obtain the total Ps formation cross sections. Comparisons with other theoretical calculations and experimental date are shown in Fig. 7. As seen from the figure, the EFS-CDW results agree with the experiment very well. So do the CC, CCC, and CCO calculations. For other distorted wave methods, the DWA [7] and SBA [6] models overestimate the experiment significantly at low energies while

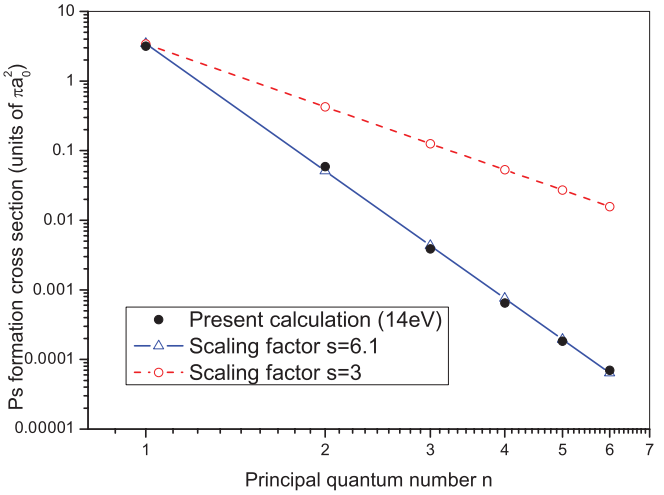

FIG. 8. (Color online) Ps (n) formation cross sections versus principal quantum number n for positron-hydrogen scattering at 14 eV.

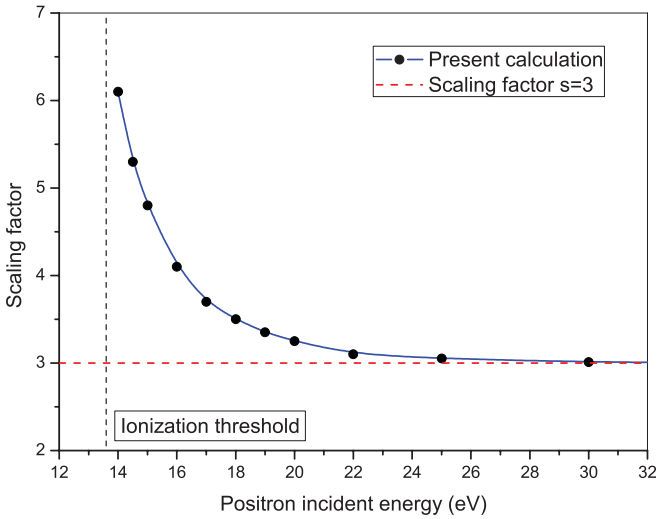

FIG. 9. (Color online) Scaling factors of the scaling law: $\sigma_{Ps}(n) \propto n^{-s}$ at different impact energies. The solid line is used to guide the eye.

the most recent SDWA [8] model corresponds to the lower limit of experiment. The PODWA [10] model underestimates the experiment at whole energies.

It is generally considered that the n^{-3} scaling law [38] for Ps (n) formations is applicable only for highly exited states such as Rydberg states [18]. However, the most recent calculations of the classical trajectory Monte-Carlo (CTMC) [39] method has predicted that at about 100 eV the scaling law is valid for all principal quantum number n. In the following discussion, we pay special attention to the scaling law for Ps (n) formations. As we can see from Fig. 7, the use of the n^{-3} scaling law for $n \geqslant 2$ states, i.e.,

$$\sigma_{Ps} = \sigma_{Ps}(1s) + \sigma_{Ps}(1s) \sum_{n=2}^{\infty} \frac{1}{n^3} = \sigma_{Ps}(1s)1.202, \quad (30)$$

indicates that such scaling law is not valid at low energies. It overestimates the total Ps formation especially at the maximum position. Assuming the n^{-3} scaling law is valid for $n \geqslant 3$ states, the CC methods use

$$\sigma_{Ps} = \sigma_{Ps}(1s) + \sigma_{Ps}(n=2) + \sigma_{Ps}(n=2)8 \sum_{n=3}^{\infty} \frac{1}{n^3} \quad (31)$$

to estimate the total Ps formation (CCC [19] does not need). Although these models have good agreement with the experimental results, it is hard to estimate the validity of the scaling law due to the relatively small contribution of the excited Ps states to the total Ps formation process.

In Fig. 8, the lowest six Ps (n) formation results calculated by the present EFS-CDW model at 14 eV are displayed against the principal quantum number n. It is surprisingly noted that these results are good in accordance with the scaling law,

$$\sigma_{Ps}(n) \propto n^{-s}, \quad (32)$$

with scaling factor $s = 6.1$. In Fig. 9 we have shown the scaling factors corresponding to the impact energies from the ionization threshold 13.6 eV, where all Ps formation channels are open, to 30 eV. As one can see, the factors start from an extrapolative value of infinity at the ionization threshold, decrease monotonously as the energy increases, and approach to a limit 3 at nearly 30 eV. Above 30 eV, the n^{-3} scaling law is well kept for all Ps (n) formation cross sections as it is predicted by the CTMC [39] calculations.

IV. CONCLUSION

In conclusion, we have successfully extended the EFS-CDW model to the Ps formation into arbitrary excited states. The Ps (n) with $n \leqslant 5$ and total Ps formation cross sections are calculated and compared with available theoretical calculations and experimental results. In comparison with other perturbation-based methods, it appears that the present EFS-CDW model is more accurate at relatively low energies. The maximum positions for Ps (n) formations are generally in accord with the wave vector matching model of Charlton [27]. In the present calculation, it has also been shown that a n^{-s} scaling law is kept for all n in the entire energy range only by adjusting the scaling factor s with the impact energy. At high energies the scaling factor expectedly approaches to the limit 3. Calculations for other targets appear as necessary to validate the scaling law. With the development of advanced experimental technologies, the direct measurement of excited Ps formation cross sections is now available for noble gas atoms [40]. We greatly expect such measurement can presumably be performed on the positron-hydrogen system in the future.

ACKNOWLEDGMENT

We are grateful for the support of this work by the National Natural Science Foundation of China under Grant No. 11174066.

[1] M. Charlton and J. W. Humberston, *Positron Physics* (Cambridge University Press, Cambridge, 2001).
[2] C. M. Surko, G. F. Gribakin, and S. J. Buckman, J. Phys. B **38**, R57 (2005).
[3] M. Weber, A. Hofmann, W. Raith, W. Sperber, F. Jacobsen, and K. G. Lynn, Hyperfine Interact. **89**, 211 (1994).
[4] S. Zhou, H. Li, W. E. Kauppila, C. K. Kwan, and T. S. Stein, Phys. Rev. A **55**, 361 (1997).
[5] M. Basu and A. S. Ghosh, J. Phys. B **21**, 3439 (1988).
[6] A. Igarashi, N. Toshima, and T. Ishihara, Phys. Rev. A **46**, 5525 (1992).
[7] A. Ghoshal and P. Mandal, Phys. Rev. A **72**, 032714 (2005).
[8] S. Sen, P. Mandal, and P. K. Mukherjee, Eur. Phys. J. D **62**, 379 (2011).
[9] P. Khan and A. S. Ghosh, Phys. Rev. A **27**, 1904 (1983).
[10] P. Khan, P. S. Mazumdar, and A. S. Ghosh, Phys. Rev. A **31**, 1405 (1985).

[11] X. J. Chen, B. Wen, Y. W. Xu, and Y. Y. Zheng, J. Phys. B **25**, 4661 (1992).
[12] B. H. Bransden, C. J. Joachain, and J. F. McCann, J. Phys. B **25**, 4965 (1992).
[13] P. A. Macri, J. E. Miraglia, J. Hanssen, O. A. Fojon, and R. D. Rivarola, J. Phys. B **37**, L111 (2004).
[14] P. A. Macri, Nucl. Instrum. Methods B **247**, 75 (2006).
[15] A. A. Kernoghany, D. J. R. Robinson, M. T. McAlinden, and H. R. J. Walters, J. Phys. B **29**, 2089 (1996).
[16] J. Mitroy, J. Phys. B **29**, L263 (1996).
[17] A. Igarashi and N. Toshima, Phys. Rev. A **50**, 232 (1994).
[18] N. Yamanaka and Y. Kino, Phys. Rev. A **64**, 042715 (2001).
[19] A. S. Kadyrov and I. Bray, Phys. Rev. A **66**, 012710 (2002).
[20] Y. J. Cheng and Y. J. Zhou (private communication).
[21] C. J. Brown and J. W. Humberston, J. Phys. B **18**, L401 (1985).
[22] K. Higgins and P. G. Burke, J. Phys. B **26**, 4269 (1993).
[23] S. Kar and P. Mandal, Phys. Rev. A **62**, 052514 (2000).
[24] P. L. Bartlett, A. T. Stelbovics, T. N. Rescigno, and C. W. McCurdy, Phys. Rev. A **77**, 032710 (2008).
[25] A. Ghoshal and P. Mandal, J. Phys. B **41**, 175203 (2008).
[26] B. H. Bransden and M. R. C. McDowell, *Charge Exchange and the Theory of Ion-Atom Collisions* (Clarendon, Oxford, 1992).
[27] M. Charlton, J. Phys. B **39**, 4575 (2006).
[28] I. M. Cheshire, Proc. Phys. Soc. **84**, 89 (1964)
[29] O. A. Fojon, R. D. Rivarola, R. Gayet, J. Hanssen, and P. A. Hervieux, Phys. Rev. A **54**, 4923 (1996).
[30] S. Jones and D. H. Madison, Phys. Rev. A **65**, 052727 (2002).
[31] R. D. Picca, J. Fiol, R. O. Barrachina, and V. D. Rodriguez, Nucl. Instrum. Methods B **247**, 52 (2006).
[32] A. Benedek and R. I. Campeanu, J. Phys. B **40**, 1589 (2007).
[33] M. Gell-Mann and M. L. Goldberger, Phys. Rev. **91**, 398 (1953).
[34] S. Jones and D. H. Madison, Phys. Rev. A **62**, 042701 (2000).
[35] M. S. Gravielle and J. E. Miraglia, Comput. Phys. Commun. **69**, 53 (1992).
[36] D. Belkic, J. Phys. B **17**, 3629 (1984).
[37] T. Hahn, Comput. Phys. Commun. **176**, 712 (2007).
[38] K. Omidvar, Phys. Rev. A **12**, 911 (1975).
[39] R. O. Barrachina, J. Fiol, and P. Macri, Nucl. Instrum. Methods B **266**, 402 (2008).
[40] D. J. Murtagh, D. A. Cooke, and G. Laricchia, Phys. Rev. Lett. **102**, 133202 (2009).